JOC The Journal of Organic Chemistry

Article

pubs.acs.org/joc

How Torsional Effects Cause Attack at Sterically Crowded Concave Faces of Bicyclic Alkenes

Steven A. Lopez,[‡] Melika Pourati,[‡] Hans-Joachim Gais,[†] and K. N. Houk*[,‡]

[‡]Department of Chemistry and Biochemistry, University of California, Los Angeles, California 90095-1569, United States

[†]Institute of Organic Chemistry, RWTH Aachen University, Landoltweg 1, 52074 Aachen, Germany

Supporting Information

ABSTRACT: Cycloadditions of 1,3-dipoles and related species to a *cis*-oxabicyclo[3.3.0]octenone occur on the more sterically crowded concave face. These cycloadditions were studied experimentally by Gais and co-workers in 1998 (*Eur. J. Org. Chem.* **1998**, 257−273) and have now been studied computationally with density functional theory (DFT). Transition states have been computed for various types of (3 + 2) cycloadditions, including diazomethane 1,3-dipolar cycloadditions, a thermally promoted methylenecyclopropane acetal cycloaddition, and a Pd-catalyzed cycloaddition of methylenecyclopropane to an oxabicyclo[3.3.0]octenone. The concave stereoselectivities arise from alkene predistortion that leads to torsional steering in the transition states.

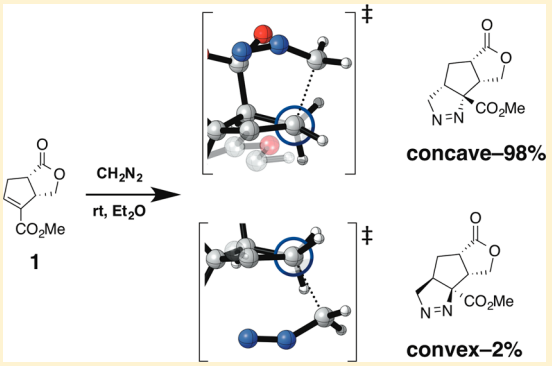

INTRODUCTION

The pentalenolactone family includes natural products with antibiotic, antiviral, and antitumor activities.[1] Gais and co-workers undertook the synthesis of pentalenolactone F, a precursor in the biosynthesis of other members of the pentalenolactone family (Figure 1).[2a] The Binger- and Trost-type palladium-catalyzed cycloadditions[3,4] were used to generate tricyclic quinanes.

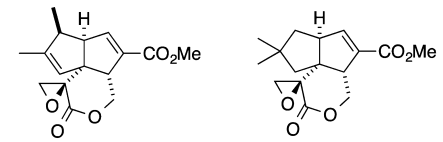

Figure 1. Pentalenolactone and pentalenolactone F.

Gais and co-workers report that the contrasteric product was unexpectedly formed for many of the reactions they performed.[2a] Scheme 1 shows the reactions of CH_2N_2, silylmethylallyl acetate, **2**, and **4** with **1** as well as reported product distributions reported by Gais and co-workers. They proposed that the stereoselectivity associated with the CH_2N_2 cycloaddition resulted from electrostatic stabilization only possible in concave transition states.[2a] We used quantum mechanical calculations to probe the origins of the stereoselectivities and evaluated these factors and others that lead to stereoselectivity in spite of obvious steric barriers to reaction.

Torsional effects have been shown to influence the manner by which a reagent adds to an unsymmetrical π bond.[8a] The selectivity typically arises from favorable torsional effects (staggering) in one transition structure and unfavorable torsional effects (eclipsing) in the other. Felkin proposed this for nucleophilic additions to carbonyls,[5] and transition state calculations have revealed the importance of these effects for stereoselective hydride reductions of ketones[6] and other types of nucleophilic attack[7] and reactions of electrophiles,[8] radicals,[9] as well as concerted cycloadditions.[8a,10]

Norbornene is a bicyclic hydrocarbon featuring a cyclopentene fixed in a pronounced envelope conformation. Huisgen discovered strong exo-stereoselectivity and rate acceleration associated with cycloadditions to the strained alkene.[11] Our group explained that the exo-stereoselectivity resulted from torsional steering.[12]

Additions to conformationally flexible cyclopentenes are more complicated, but addition is generally preferred to the concave face of the envelope cyclopentene.[13] Overman reported a contrasteric OsO_4 dihydroxylation that occurs from the concave face of a [3.3.0] bicycle, and our group determined that torsional effects direct that and related concave dihydroxylations.[14] Figure 2 shows 3,4-fused cyclopentenes studied by Danishefsky (epoxidations)[13] and Overman (OsO_4).[14]

COMPUTATIONAL METHODS

All computations were carried out with the GAUSSIAN 09 series of programs.[15] Stationary points for the Pd-catalyzed (3 + 2) cycloadditions were computed using the M06[16] level of theory with the LANL2DZ[17] pseudopotential for Pd and the 6-31G+(d,p) basis set for

Received: July 14, 2014
Published: July 28, 2014

   dx.doi.org/10.1021/jo501557z | J. Org. Chem. 2014, 79, 8304−8312

Scheme 1. Experimental Conditions and Product Ratios for the (3 + 2) Cycloadditions with Diazomethane (first row), Methylenecyclopropane 2 (second row), Silylmethylallyl Acetate, and Methylenecyclopropane Acetal 3 (fourth row).[2a]

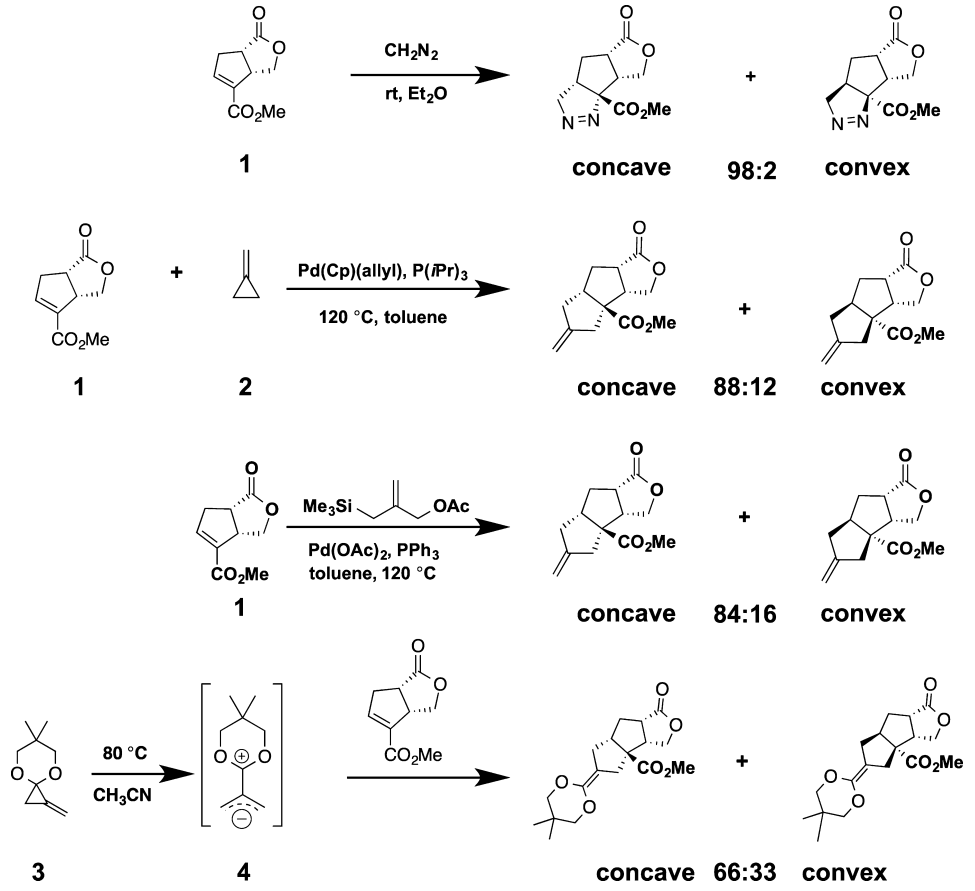

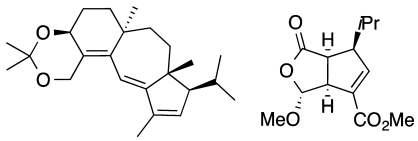

Figure 2. 3,4-Fused cyclopentenes studied by Danishefsky and Overman.

all other atoms in the gas phase. Single-point energy calculations on these geometries were performed using M06/6-311+G(d,p). The single-point calculations include solvation by toluene using the integral equation formalism polarizable continuum model (IEFPCM).[18]

The stationary points corresponding to the CH_2N_2 and methylenecyclopropane acetal cycloadditions were optimized employing M06-2X[19] and the double-ζ split-valence 6-31+G(d,p) basis set. Some transition states for the methylenecyclopropane acetal could not be located with gas-phase calculations. It has been shown that polarizable continuum models are sometimes necessary to locate stationary points in polar media; it does not significantly alter frequencies.[20] Therefore, M06-2X/6-31+G(d,p) IEFPCM^{MeCN} was utilized for optimizations for the computations involving methylenecyclopropane acetal. Single-point energy calculations on the diazomethane and methylenecyclopropane acetal stationary points were carried out using M06-2X/6-311+G(d,p) IEFPCM^{Et2O} and M06-2X/6-311+G(d,p) IEFPCM^{MeCN}, respectively.

All optimizations used tight convergence criteria, and an ultrafine grid was used throughout this work for numerical integration of density.[21] Vibrational analysis confirmed all stationary points to be minima (no imaginary frequencies) or first-order saddle points (one imaginary frequency). Thermal corrections were computed from unscaled frequencies for a standard state of 298.15 K and 1 atm. Truhlar's quasiharmonic approximation correction was applied to all optimizations, which sets frequencies less than 100 to 100 cm^{-1} for thermal corrections and entropies.[22]

RESULTS/DISCUSSION

The computed structures of the global minimum, a conformer of bicyclic lactone **1**, and the crystal structure[2a,23] of **1-CS** are shown in Figure 3. The C_4 of the cyclopentene moiety is "up" in the global minimum and "down" in conformer **1-down**. The dihedral angle formed by $C_1C_2C_3C_4$ is constrained to 10° below the plane of the cyclopentene moiety. Figure 3 shows Newman projections of fully optimized **1** and a constrained **1-down** looking down the highlighted bond. **1-down** is not the global minimum, since it produces eclipsing along the green bond.

1-down is 3.5 kcal mol^{-1} above **1** and collapses to **1** upon unconstrained optimization. The global minimum shows the sp^2 vinylic carbons attached to the ester are pyramidalized by 4° in the convex direction. The structure of **1** was determined by X-ray crystallography, and the alkene is indeed pyramidalized 4° in the convex direction.[2a] The computed structure is nearly identical to that resolved by X-ray crystallography. However, the crystal structure shows the ester and alkene in an *s-cis* configuration. We compute the *s-cis* configuration of **1** to be 0.3 kcal mol^{-1} above the *s-trans* configuration.

The transition structures for addition of CH_2N_2 on the concave and convex faces of **1** were located (**TS1-conc** and **TS-conv**, respectively). The transition structures involve nucleophilic attack of the diazomethane carbon terminus on the β-

dx.doi.org/10.1021/jo501557z | J. Org. Chem. 2014, 79, 8304−8312

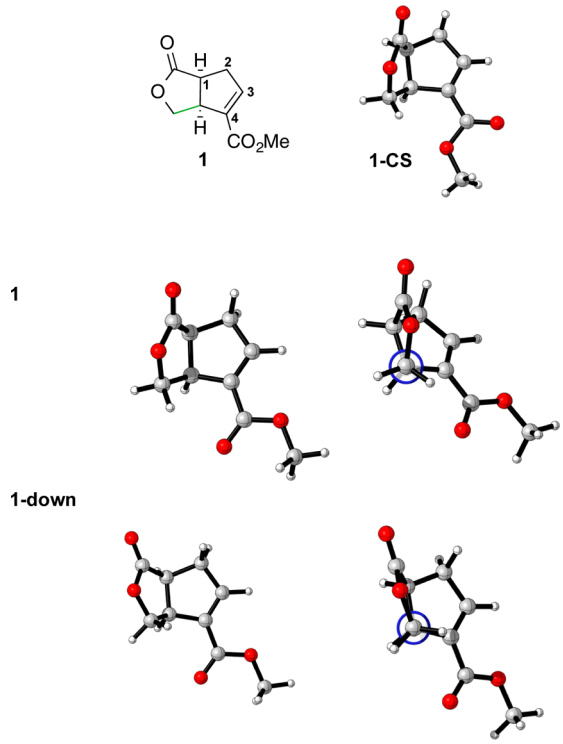

Figure 3. (Left) Geometries of **1** and **1-down**. (Right) Newman projections looking down the highlighted bond for **1** and **1-down**. Computed at the M06-2*X*/6-31+G(d,p) level of theory.

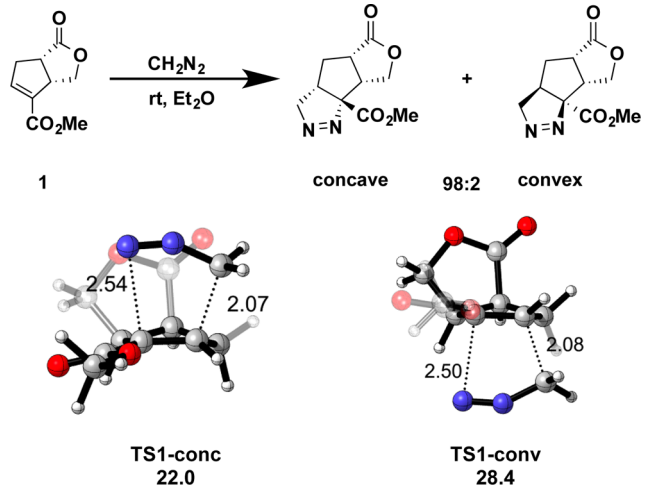

Figure 4. Optimized transition structures for concave and convex attack of CH_2N_2 on **1**. Bond lengths are reported in Angstroms. Computed at the M06-2X/6-311+G(d,p) IEFPCM^{Et2O}//M06-2X/6-31+G(d,p) level of theory. Activation free energies are reported in kcal mol^{-1}.

carbon of the α,β-unsaturated ester. The other regioisomeric transition structures were located but are much higher in energy. Figure 4 shows the lowest energy transition structures and computed activation free energies.

The transition structures reflect the polar nature of the ester on the double bond of **1**; they are concerted but asynchronous. Both concave transition structures have shorter forming C−C bond lengths than C−N bond lengths (2.07 and 2.08 Å vs 2.54 and 2.50 Å, respectively). **TS1-conc** is lower in free energy than **TS1-conv** by 6.4 kcal mol^{-1}. This is an overestimation of the

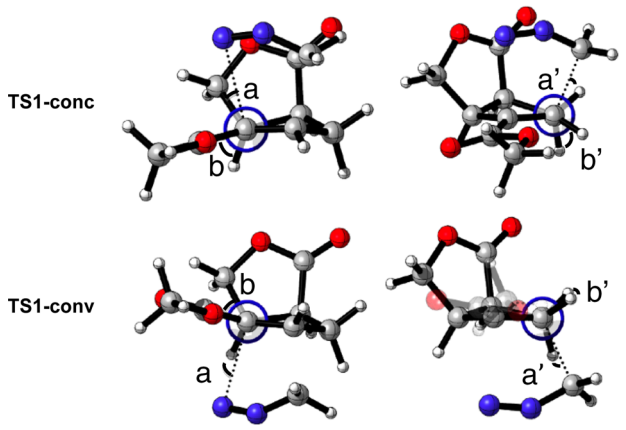

Figure 5. Newman projections looking down the alkene−allylic C−C bonds of **TS1-conc** are shown in the top row, and those for **TS1-conv** are shown in the bottom row. Computed at the M06-2X/6-31+G(d,p) level of theory.

Scheme 2. Theoretical Reaction of 1a with CH_2N_2

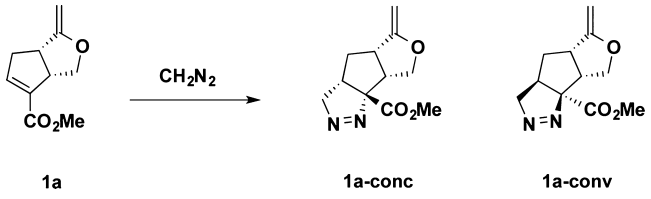

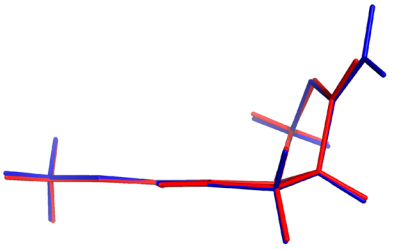

Figure 6. Overlaid geometries of reactants **1** (red) and **1a** (blue). Computed at the M06-2X/6-31+G(d,p) level of theory.

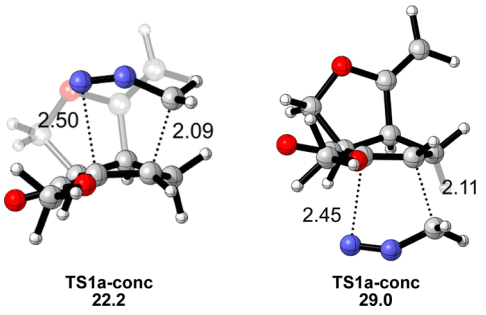

Figure 7. Transition structures for the 1,3-dipolar cycloaddition of CH_2N_2 and **1a**. Activation free energies are computed at the M06-2X/6-311+G(d,p) IEF-PCM^{Et2O}//M06-2X/6-31+G(d,p) level of theory. Values are activation free energies and reported in kcal mol^{-1}. Bond lengths are given in Angstroms.

concave:convex substantial stereoselectivity (98:2), but the calculations do reflect great concave stereoselectivity.

The distortion/interaction model was used to analyze the origins of diazomethane cycloaddition stereoselectivity. The activation energy ($\Delta E^{\ddagger}$) is dissected into distortion energy

dx.doi.org/10.1021/jo501557z | J. Org. Chem. 2014, 79, 8304−8312

Scheme 3. Product Ratios Found for Reactions of 1b and 1c with CH_2N_2[2a]

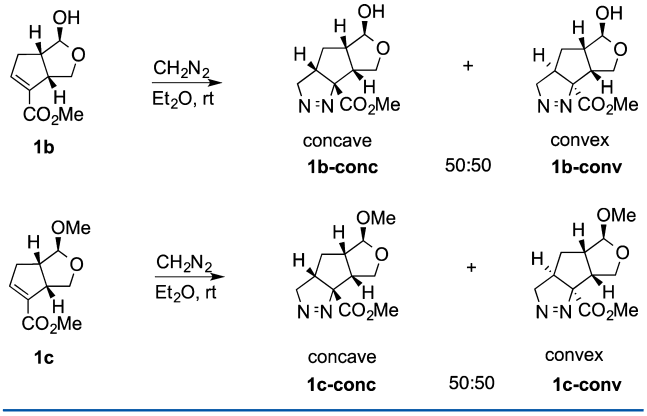

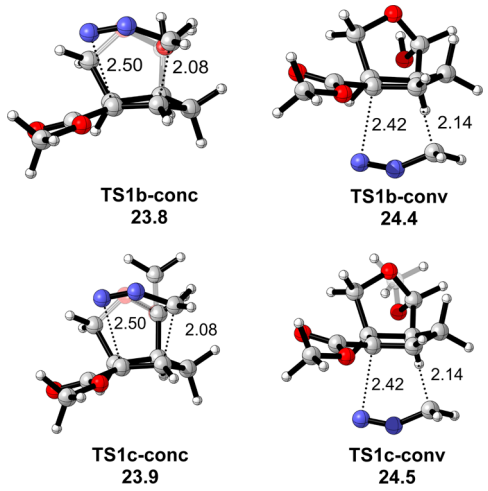

Figure 9. 1,3-Dipolar cycloaddition transition structures for reactions of diazomethane with **1b** and **1c**. Bond lengths are reported in Angstroms. Activation free energies computed at the M06-2X/6-311+G(d,p) IEF-PCM^{Et2O}//M06-2X/6-31+G(d,p) level of theory. Energies are reported in kcal mol^{-1}.

($\Delta E_d^{\ddagger}$) and interaction energy ($\Delta E_i^{\ddagger}$).[24] Distortion energy is the energy required to distort each of the reactants into their respective transition state geometries without allowing them to interact. The interaction energy is the energy of interaction between the destabilized cycloaddends. It is often a net stabilizing quantity that results from charge transfer from occupied−vacant orbital interactions, electron transfer, polarization, and closed-shell (steric) repulsions.

The distortion energies of **TS1-conc** and **TS1-conv** are 24.6 and 26.1 kcal mol^{-1}, respectively. The interaction energies are −18.8 and −13.4 kcal mol^{-1}, respectively. $\Delta\Delta E_i^{\ddagger}$ is larger than $\Delta\Delta E_d^{\ddagger}$ and mainly responsible for the stereoselectivity. We evaluated torsional effects in **TS1-conc** and **TS1-conv** using Newman projections, which are shown in Figure 5.

Newman projections of **TS1-conc** show partially staggered newly forming C−N and C−C bonds (a and a′ = 20° and 26°, respectively). The newly forming C−N bonds are almost perfectly eclipsed in **TS1-conv** (a and a′ = 9° and 10°, respectively). This torsional strain in **TS1-conv** manifests itself as reduced interaction energy because the eclipsing occurs between the two reacting cycloaddends (−18.8 vs −13.4 kcal mol^{-1}, respectively). The vicinal ester-CC−CH_2 and HCCH bonds are staggered in **TS1-conc** (b and b′ = 56° and 48°), while these are nearly eclipsed in **TS1-conv** (b and b′ = 47° and 15°). Since **1** must distort into a conformation with eclipsed vicinal C−H bonds to reach the convex transition structures, this torsional strain is reflected as increased distortion energy (24.6 and 26.1 kcal mol^{-1}).

Gais and co-workers proposed that electrostatic interaction between the nucleophilic carbon terminus of CH_2N_2 and the electrophilic lactone carbon in **1** stabilizes **TS1-conc** and not **TS1-conv**.[2a] We evaluated this hypothesis by computing the reaction of **1a** with CH_2N_2 (Scheme 2). **1a** differs from **1** only in that the carbonyl oxygen in **1** is replaced with a methylene group in **1a**. The global minima of **1** (red) and **1a** (blue) are overlaid in Figure 6 to compare their ground state structures.

These structures are nearly identical and are in a fixed envelope conformation. The vinyl ester is pyramidalized in the convex direction by 4° in both **1** and **1a**. Figure 7 shows the transition states for attack of CH_2N_2 on the concave and convex faces of **1a**. Activation free energies are shown below each structure.

Despite greatly reducing the potential electrostatic stabilization of the concave transition states, the reaction is still predicted to be highly concave stereoselective ($\Delta\Delta G^{\ddagger}$ = 6.7 kcal mol^{-1}). Our computations show that electrostatic stabilization of the concave transition structures is not responsible for concave stereoselectivity, but torsional effects do explain stereoselectivity. Gais and co-workers found that the reactions of CH_2N_2 with hemiacetal **1b** and acetal **1c** are nonstereoselective (Scheme 3).[2a] We computationally investigated the origins of the low selectivities of CH_2N_2 cycloadditions to **1b** and **1c**.

Figure 8 shows an overlay of the global minima of **1b** (orange) and **1c** (green), and another overlay compares the structures of **1c** (green) and **1** (red).

Figure 8 shows that **1b** and **1c** are nearly identical in structure and feature planar cyclopentene moieties. **1** prefers an envelope conformation, a predistortion that makes it resemble the concave addition. Figure 9 shows the transition structures for the 1,3-dipolar cycloadditions of CH_2N_2 with **1b** and **1c**. We also computed the transition structures for two other configurations of the OH and OMe in **1b** and **1c**, respectively

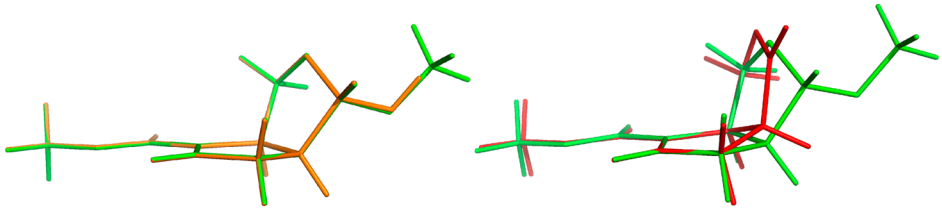

Figure 8. Overlay of **1b** (orange) and **1c** (green) is shown on the left side, and overlay of **1** (red) and **1c** (green) is shown on the right side. Computed at the M06-2X/6-31+G(d,p) level of theory.

dx.doi.org/10.1021/jo501557z | J. Org. Chem. 2014, 79, 8304−8312

Scheme 4. (a) Disrotatory Electrocyclic Ring Opening Reaction; (b) Stepwise Pathway Involving Zwitterionic Intermediate 4

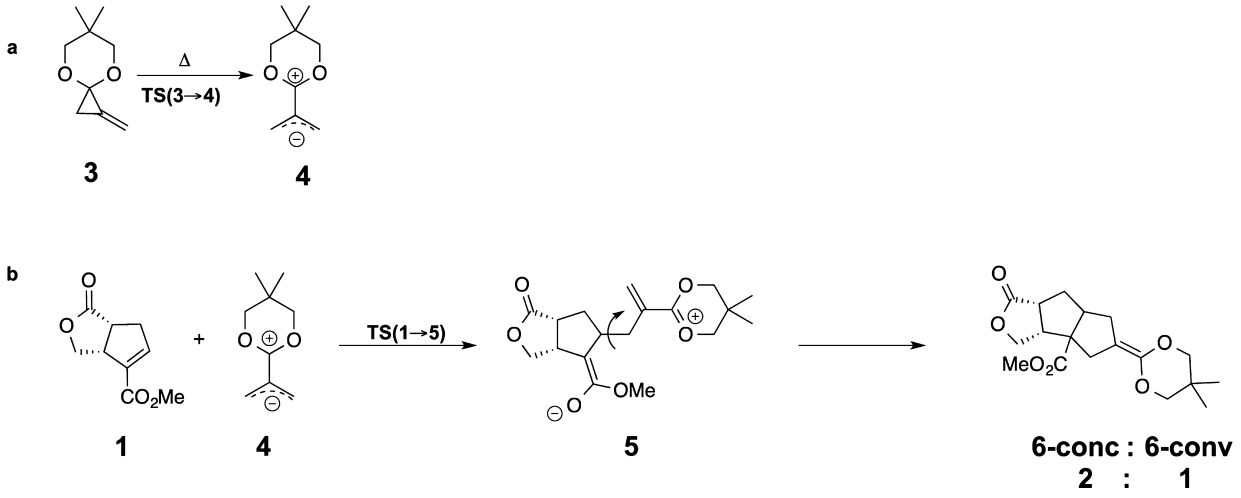

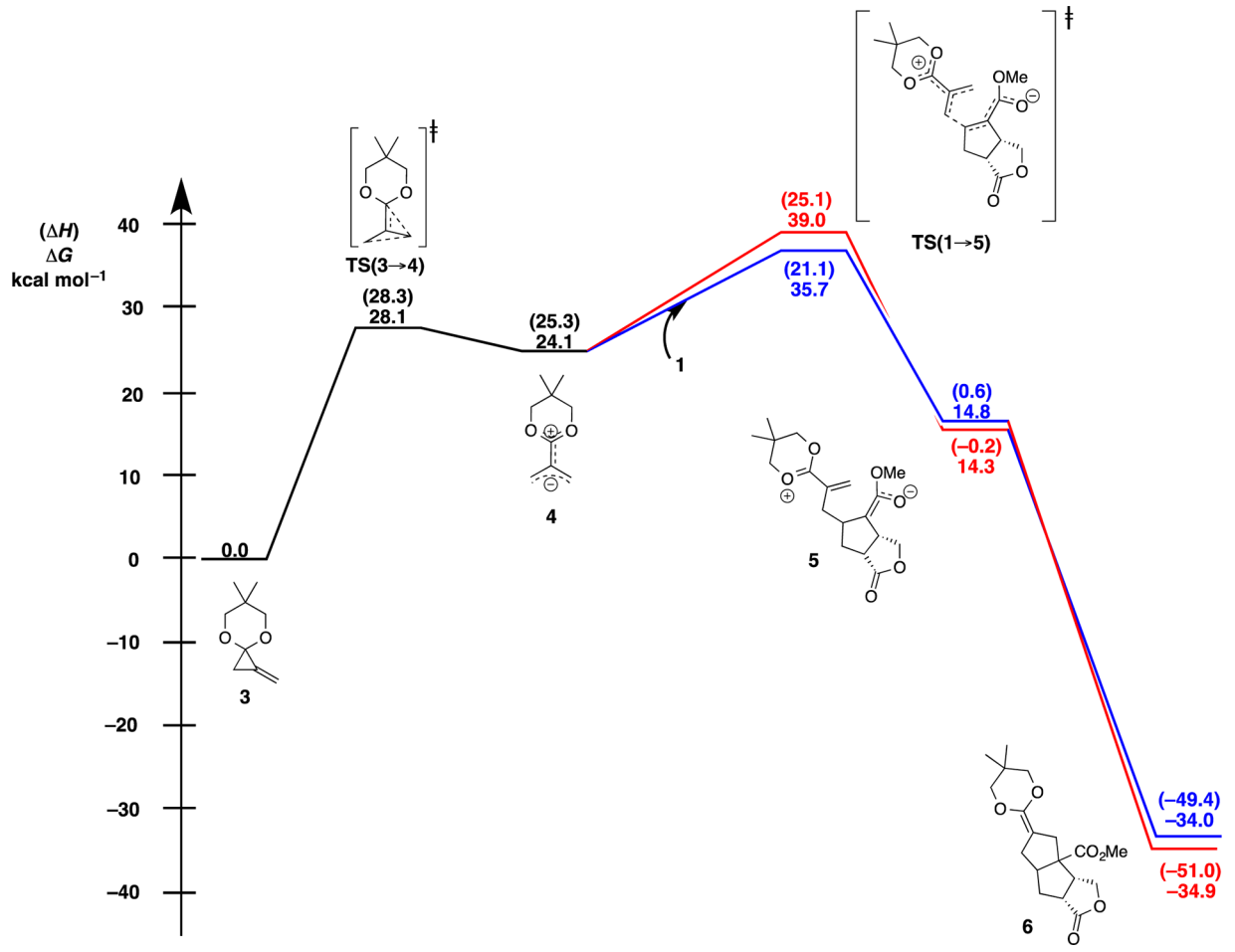

Figure 10. Computed free energy profile for the stepwise pathway of concave (blue) and convex (red) additions to **1**. Energies reported in black correspond to ring opening of **3**. Free energies and enthalpies are reported in kcal mol^{-1} and relative to **1** and **3**. Computed at the M06-2X/6-311+G(d,p) IEF-PCM^{MeCN}//M06-2X/6-31+G(d,p) IEF-PCM^{MeCN} level of theory.

(coordinates and energies can be found in the Supporting Information). These structures are 1.7−3.1 kcal mol^{-1} higher in energy than those shown in Figure 9.

The computed activation free energies show a preference for cycloadditions to the concave face for **1b** and **1c** of only 0.6 kcal mol^{-1} in both cases. Although these results suggest a slight preference for attack on the concave face of **1b** and **1c**, $\Delta\Delta G^{\ddagger}$ values are very small.

Methylenecyclopropane Acetal Cycloadditions. Cycloadditions of methylenecyclopropane acetals were first performed by Yamago and Nakamura in 1989.[25] Thermolysis causes a 2π disrotatory electrocyclic ring opening[26] of methylenecyclopropane acetals to generate the zwitterionic

dx.doi.org/10.1021/jo501557z | J. Org. Chem. 2014, 79, 8304−8312

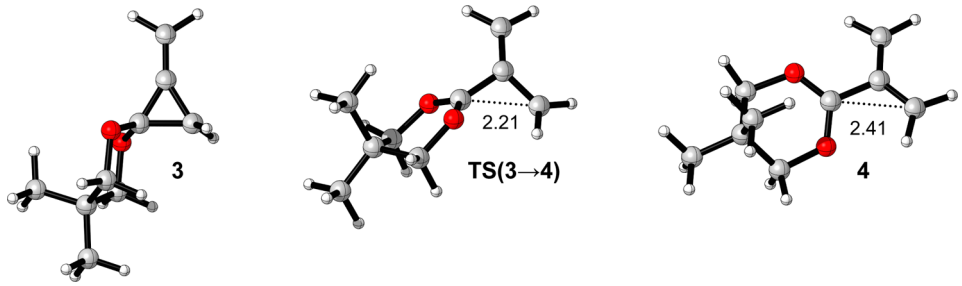

Figure 11. Geometries of methylenecyclopropane acetal **3**, ring-opening transition state [**TS(3 → 4)**], and reactive intermediate **4**. Bond lengths are reported in Angstroms. Computed at the M06-2X/6-31+G(d,p) IEF-PCM^{MeCN} level of theory.

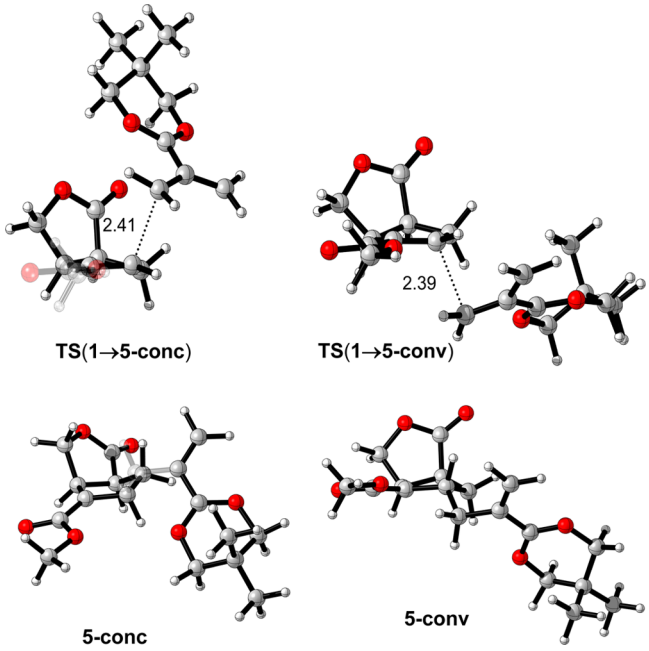

Figure 12. Stepwise transition structures for addition of **4** and **1** and corresponding zwitterionic intermediates. Bond lengths are reported in Angstroms. Computed at the M06-2X/6-31+G(d,p) IEF-PCM^{MeCN} level of theory.

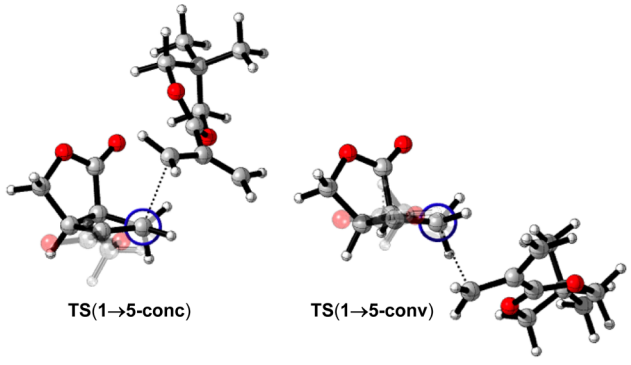

Figure 13. Newman projections of **TS(1 → 5-conc)** and **TS(1 → 5conv)**. Calculated at the M06-2X/6-31+G(d,p) level of theory. The methyl ester is hidden for clarity.

1,3-dipole **4**. Previous computational studies showed that the most stable form of the dipole is the closed-shell singlet species.[27] Experimentally, the cycloadditions follow the "endo rule", and a highly polar transition state has been proposed.[28] Scheme 4a shows the electrocyclic ring opening of **3** to form **4**, and Scheme 4b shows the subsequent stepwise addition of **4** to **1**. Gais and co-workers report that the concave:convex product ratio is 2:1.[2a]

Figure 10 shows the free energy profile for the mechanism shown in Scheme 4. The energies are relative to separated reactants (**1** and **3**). The computed structures of relevant species from Scheme 4 are shown in Figures 11 and 12.

Formation of reactive intermediate **4** is highly endergonic (ΔG = 24.1 kcal mol^{-1}). No transition states for a concerted cycloaddition of **4** and **1** at various levels were located. In line with this, a two-dimensional relaxed scan of the potential energy surface suggested the concerted process was barrierless. This is because of the negative enthalpic barriers for **TS(1 → 5-conc)** and **TS(1 → 5-conv)**, −4.2 and −0.2 kcal mol^{-1}, respectively. Therefore, a variational transition state treatment is required to determine $\Delta\Delta G^{\ddagger}$ for this reaction more accurately.

Transition structures corresponding to stepwise addition of **4** to **1** [**TS(1 → 5-conc)** and **TS(1 → 5-conv)**] were located and found to be only 11.6 and 14.9 kcal mol^{-1} higher in free energy than **4** and **1**, respectively, and in fact lower in ΔH than separated reactants **4** and **1**. Stepwise addition to the concave face is preferred (35.7 kcal mol^{-1}) to the convex face addition (39.0 kcal mol^{-1}). The $\Delta\Delta G^{\ddagger}$ between **TS(1 → 5-conc)** and **TS(1 → 5-conv)** is 3.3 kcal mol^{-1}, a significant overestimation of $\Delta\Delta G^{\ddagger}$ that corresponds to the experimentally observed concave:convex product ratio (2:1). These computed transition structures and the resulting zwitterionic intermediates (**5-conc** and **5-conv**) are shown in Figure 12.

TS(1 → 5-conc) and **TS(1 → 5-conv)** have newly forming C−C bond lengths of 2.41 and 2.39 Å, respectively. In line with the analysis done for the CH_2N_2 cycloadditions, we evaluated the torsional effects in **TS(1 → 5-conc)** and **TS(1 → 5-conv)** using Newman projections looking along the C_2−C_3 bond of the cyclopentene moiety (Figure 13).

Figure 13 shows staggering of HCCH bonds (vinyl H−methylene H) in **TS(1 → 5-conc)** and eclipsing of the same bonds in **TS(1 → 5-conv)**. Despite the increased size and mechanistic complexity of this reaction as compared to the CH_2N_2 cycloaddition, torsional effects are responsible for concave stereoselectivity.

Pd-Catalyzed (3 + 2) Cycloaddition. Pd-catalyzed (3 + 2) reactions involving methylenecyclopropane **2** afford synthetically useful fused cyclopentanes.[29] The cycloadditions of methylenecyclopropanes with electron-deficient alkenes have been shown to be catalyzed by Pd and Ni.[4,30] Previous computational mechanistic studies of intramolecular Pd-catalyzed (3 + 2) cycloadditions were done by Cárdenas et al. and include an alternate mechanism involving a σ-allyl palladium complex.[31] Those results guided our computations that lead to the most favorable mechanism (Scheme 5). Our

dx.doi.org/10.1021/jo501557z | J. Org. Chem. 2014, 79, 8304−8312

Scheme 5. Mechanism of Pd-Catalyzed (3 + 2) Cycloaddition Computed Here

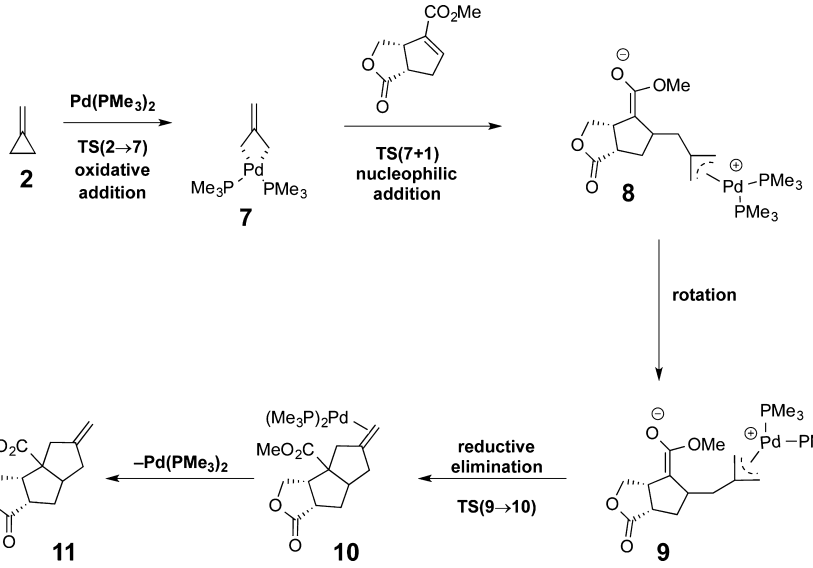

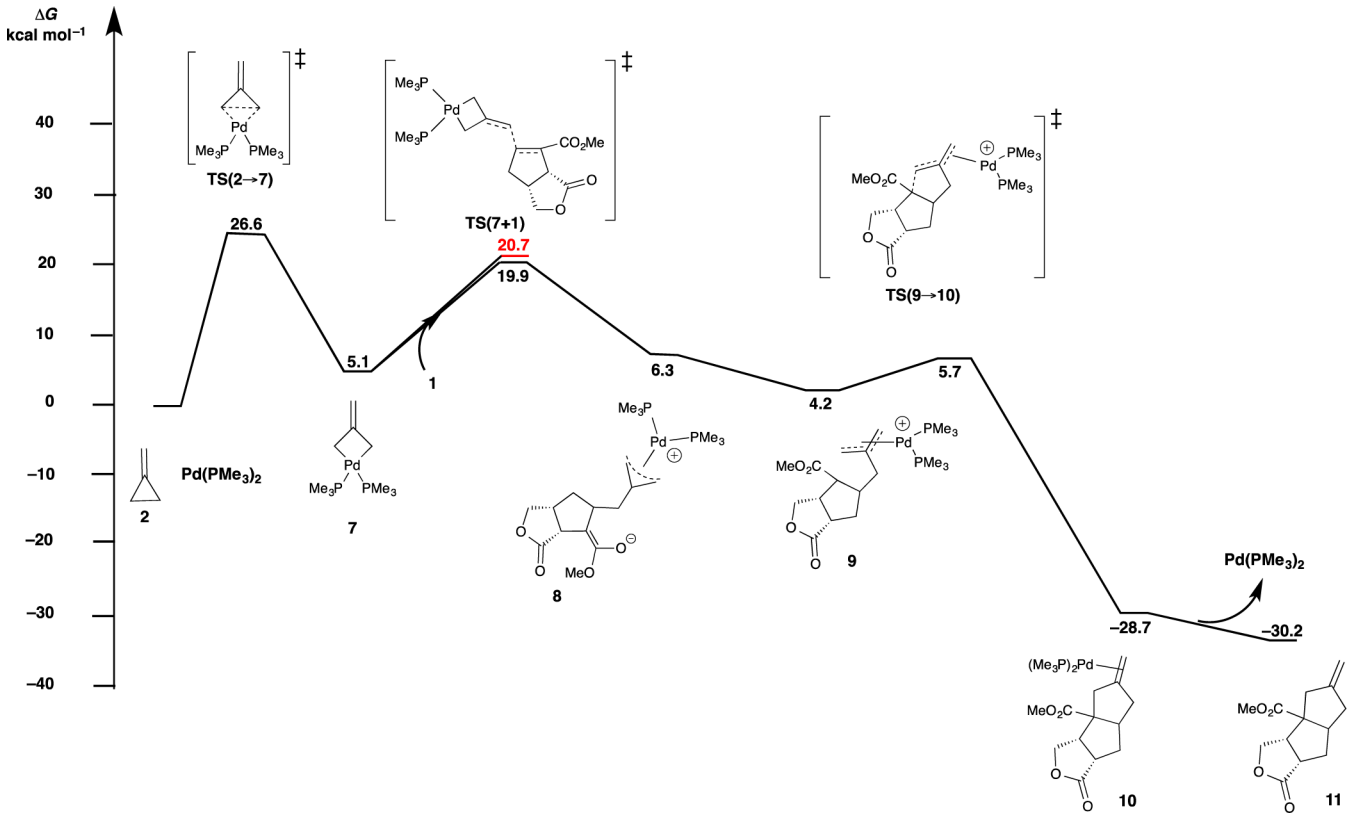

Figure 14. Free energy profile for the mechanism for the Pd-catalyzed (3 + 2) cycloaddition of **1** with **2** and $Pd(PMe_3)_2$. Values are reported in kcal mol^{-1} and relative to separated **1**, **2**, and $Pd(PMe_3)_2$. All energies are computed at the M06/LANL2DZ-/6-311+G(d,p) IEF-$PCM^{toluene}$//M06/LANL2DZ−6-31+G(d,p) level of theory.

computational results utilize PMe_3 instead of the experimental ligand, $P(iPr)_3$; this approximation does not change the conclusions of this study. A mechanism involving coordination to the enolate oxygen of **9** was found to be higher in energy and discarded. The geometries and energies of relevant stationary points for the alternate mechanism are given in the Supporting Information.

Gais and co-workers generated the catalyst by treating [Pd(Cp)(allyl)] with $P(iPr_3)$ at −78 °C.[2a] Fujimoto reported that Pd(0) preferentially oxidatively inserts into the distal σ bond of methylenecyclopropane to form TMM−PdL_2 complex 7.[32] Figure 14 shows the free energy profile for the mechanism shown in in Scheme 5. The reported energies correspond to stationary points resulting from concave additions. The $\Delta\Delta G^{\ddagger}$ between the concave and the convex nucleophilic addition transition states will be discussed to continue our investigations of stereoselectivity. The other stationary points corresponding to addition to the convex face are not shown in Figure 15, but

dx.doi.org/10.1021/jo501557z | J. Org. Chem. 2014, 79, 8304−8312

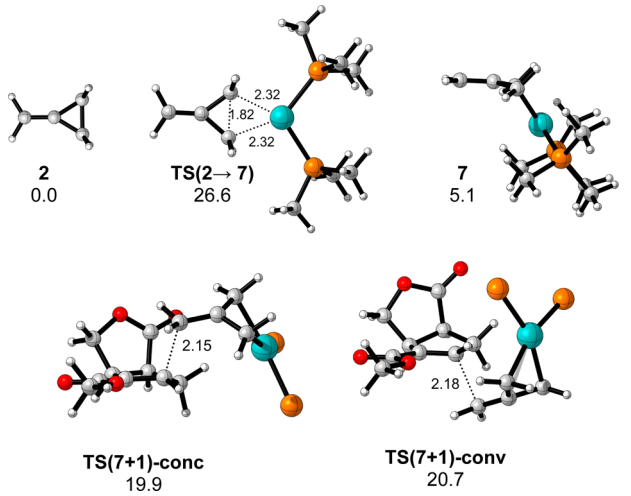

Figure 15. Computed geometries for the oxidative and nucleophilic addition steps. Computed at the M06/LANL2DZ-6-31+G(d,p) level of theory. Bond lengths are reported in Angstroms. Values are free energies and reported in kcal mol^{-1}. $-Me_3$ groups are hidden for clarity.

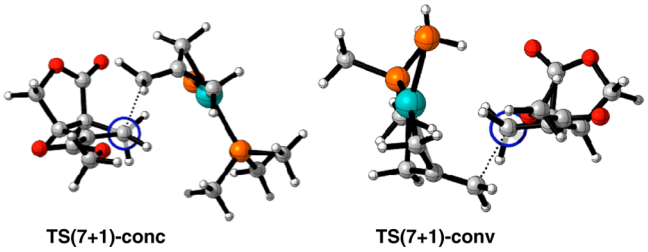

Figure 16. Newman projections of **TS(7 + 1)-conc** and **TS(7 + 1)-conv**. Calculated at the M06/LANL2DZ-6-31+G(d,p) level of theory. One of the PMe_3 groups is hidden for clarity in each structure.

the geometries and energies are given in the Supporting Information.

The oxidative addition step is rate determining ($\Delta G^{\ddagger}$ = 28.9 kcal mol^{-1}), and the four-membered palladacycle **7** is formed endergonically (ΔG = 5.1 kcal mol^{-1}). Then **7** adds nucleophilically to the concave or convex face of **1** [**TS(7 + 1)-conc** and **TS(7 + 1)-conv**, respectively]. **TS(7 + 1)-conc** is lower in energy than **TS(7 + 1)-conv** by 0.8 kcal mol^{-1}. This $\Delta\Delta G^{\ddagger}$ is a slight underestimation of the concave:convex product (7:1) ratio observed by Gais and co-workers.[2a] The large exergonicity of the overall reaction indicates that product formation is irreversible and the selectivity is under kinetic control. The stationary points leading up to and including the stereodetermining step are shown in Figure 13. The free energies are relative to **1**, **2**, and $Pd(PMe_3)_2$ and shown below each structure.

We utilized Newman projections to evaluate torsional effects in **TS(7 + 1)-conc** and **TS(7 + 1)-conv** to probe the origins of the concave stereoselectivity for this reaction. Figure 16 shows the Newman projections looking down the C_2-C_3 C−C bond of **1** in **TS(7 + 1)-conc** and **TS(7 + 1)-conv**.

The Newman projection for **TS(7 + 1)-conc** shows both allylic C−H bonds and newly forming C−C bonds are almost perfectly staggered. Conversely, **TS(7 + 1)-conv** shows some eclipsing of both allylic C−H bonds and the newly forming C−C bonds. The torsional strain is visible in the Newman projection of **TS(7 + 1)-conv** and indicates that the concave stereoselectivity arises from torsional effects in the transition state.

CONCLUSION

We determined the origins of concave stereoselectivity for cycloadditions to an oxabicyclo[3.3.0]octenone. The torsional effects are different on the two faces when the alkene is in a rigid envelope conformation.[8a] The π bond of **1** is pyramidalized 4° in the convex direction, which causes the alkene to be predistorted and resemble concave-attack transition structures. Less distortion energy is required to reach the geometry of the concave-attack transition structures, a result of favorable torsional effects. The convex transition structures are disfavored because the alkene must undergo additional distortion to overcome predistortion and achieve the geometries of convex-attack transition structures. In addition, qualitative inspection of the convex transition structures shows that torsional strain manifests itself as both decreased interaction energy and increased distortion energies in these transition structures. This effect is general to the three types of reactions studied experimentally by Gais and co-workers and here through quantum mechanical calculations.

ASSOCIATED CONTENT

Supporting Information

Calculated geometries and energies were performed using M06 and M06-2X, respectively; complete reference for Gaussian 09. This material is available free of charge via the Internet at http://pubs.acs.org.

AUTHOR INFORMATION

Corresponding Author

*E-mail: houk@chem.ucla.edu

Notes

The authors declare no competing financial interest.

ACKNOWLEDGMENTS

We thank Peng Liu, Buck Taylor, and Ashay Patel for helpful comments and the National Science Foundation (NSF CHE-1059084) for financial support of this research. This work was made possible by computer resources supplied by the Extreme Science and Engineering Discovery Environment (XSEDE), which is supported by National Science Foundation grant number OCI-10535. Figures 3−5, 7, 9, 11−13, 15 , and 16 were generated using CYLview.[33]

REFERENCES

(1) (a) Lambeir, A. M.; Loiseau, A. M.; Kuntz, D. A.; Vellieux, F. M.; Michels, F. M.; Operdoes, F. R. *Eur. J. Biohem.* **1991**, *198*, 429. (b) Braxenthaler, M.; Pötsch, B.; Fröhlich, K. U.; Dieter, M. *FEMS Microbiol. Lett.* **1991**, *83*, 311. (c) Willson, M.; Lauth, N.; Perie, J.; Callens, M.; Opperdoes, F. R. *Biochemistry* **1994**, *33*, 214. (d) Cane, D. E.; Sohng, J.-K. *Biochemistry* **1994**, *33*, 6524. (e) Lesburg, C. A.; Lloyd, M. D.; Cane, D. E.; Christianson, D. W. *Protein Sci.* **1995**, *4*, 2436. (f) Fröhlich, K.-U.; Kannwischer, R.; Rüdiger, M.; Mecke, D. *Arch. Microbiol.* **1996**, *165*, 179. (g) Spanevello, R. A.; Pellegrinet, S. C. *Cur. Top. Phytochem.* **2000**, *3*, 225. (h) Testero, S. A.; Spanvello, R. A. *Org. Lett.* **2006**, *8*, 3793. (i) Zhu, D.; Seo, M. J.; Ikeda, H.; Cane, D. E. *J. Am. Chem. Soc.* **2011**, *133*, 2128. (j) Liu, Q.; Yue, G.; Wu, N.; Lin, G.; Li, Y.; Quan, J.; Li, C.-C.; Wang, G.; Yang, Z. *Angew. Chem.* **2012**, *124*, 12238; *Angew. Chem., Int. Ed.* **2012**, *51*, 12072.

(2) (a) Rosenstock, B.; Gais, H.-J.; Herrmann, E.; Raabe, G.; Binger, P.; Freund, A.; Wedemann, P.; Krüger, C.; Linder, H. J. *Eur. J. Org.*

Chem. **1998**, 257. (b) Herrmann, E.; Gais, H.-J.; Rosenstock, B.; Raabe, G.; Lindner, H. J. *Eur. J. Org. Chem.* **1998**, 275.
(3) (a) Trost, B. M. *Pure Appl. Chem.* **1988**, *60*, 1615. (b) Trost, B. M. *Angew. Chem.* **1986**, *98*, 1. (c) Trost, B. M. *Angew. Chem., Int. Ed. Engl.* **1986**, *25*, 1. (d) Trost, B. M.; Lam, T. M.; Herbage, M. A. *J. Am. Chem. Soc.* **2013**, *135*, 2459.
(4) Binger, P.; Bücg, H. M. *Topp. Curr. Chem.* **1987**, *135*, 77.
(5) Cherest, M.; Felkin, H. *Tetrahedron Lett.* **1968**, *9*, 2205.
(6) (a) Houk, K. N.; Paddon-Row, M. N.; Rondan, N. G.; Wu, Y.-D.; Brown, F. K.; Spellmeyer, D. C.; Metz, J. T.; Li, Y.; Loncharich, R. J. *Science* **1986**, *231*, 1108. (b) Mukherjee, D.; Wu, Y.-D.; Fronczek, F. R.; Houk, K. N. *J. Am. Chem. Soc.* **1988**, *110*, 3328. (c) Ando, K.; Houk, K. N.; Busch, J.; Menasse, A.; Sequin, U. *J. Org. Chem.* **1998**, *63*, 1761.
(7) (a) Wu, Y.-D.; Houk, K. N. *J. Am. Chem. Soc.* **1987**, *109*, 908. (b) Ando, K.; Condroski, K. R.; Houk, K. N.; Wu, Y.-D.; Lu, S. K.; Overman, L. E. *J. Org. Chem.* **1998**, *63*, 3196. (c) Im, G-Y. J.; Bronner, S. M.; Goetz, A. E.; Paton, R. S.; Cheong, P. H.-Y.; Houk, K. N.; Garg, N. K. *J. Am. Chem. Soc.* **2010**, *132*, 17933. (d) Wu, Y.-D.; Houk, K. N.; Paddon-Row, M. N. *Angew. Chem., Int. Ed. Engl.* **1992**, *31*, 1019.
(8) (a) Wang, H.; Houk, K. N. *Chem. Sci.* **2014**, *5*, 462. (b) Kaori, A.; Green, N. S.; Li, Y.; Houk, K. N. *J. Am. Chem. Soc.* **1999**, *121*, 5334. (c) Lucero, M. J.; Houk, K. N. *J. Org. Chem.* **1998**, *63*, 6973.
(9) (a) Paddon-Row, M. N.; Spellmeyer, D. C.; Houk, K. N. *J. Org. Chem.* **1986**, *51*, 2874. (b) Liu, J.; Houk, K. N. *J. Org. Chem.* **1998**, *63*, 8565. (c) Damm, W.; Giese, B.; Hartung, J.; Hasskerl, T.; Houk, K. N.; Hueter, O.; Zipse, H. *J. Am. Chem. Soc.* **1992**, *114*, 4067.
(10) (a) Iafe, R. G.; Houk, K. N. *Org. Lett.* **2006**, *8*, 3469. (b) Lopez, S. A.; Houk, K. N. *J. Org. Chem.* **2013**, *78*, 1778.
(11) Huisgen, R.; Ooms, P. H. J.; Mingin, M.; Allinger, N. L. *J. Am. Chem. Soc.* **1980**, *102*, 3951.
(12) Rondan, N. G.; Paddon-Row, M. N.; Caramella, P.; Mareda, J.; Mueller, P. H.; Houk, K. N. *J. Am. Chem. Soc.* **1982**, *104*, 4974.
(13) Cheong H-Y, P.; Yun, H.; Danishefsky, S. J.; Houk, K. N. *Org. Lett.* **2006**, *8*, 1513.
(14) Wang, H.; Kohler, P.; Overman, L. E.; Houk, K. N. *J. Am. Chem. Soc.* **2012**, *134*, 16054.
(15) Frisch, M. J.; et al. *Gaussian 09*, revision C-01; Gaussian Inc.: Wallingford, CT, 2009 (see complete reference in the Supporting Information).
(16) Zhao, Y.; Truhlar, D. G. *Theor. Chem. Acc.* **2008**, *120*, 215.
(17) Hay, P. J.; Wadt, W. R. *J. Chem. Phys.* **1985**, *82*, 299.
(18) Cances, E.; Mennucci, B.; Tomasi, J. *J. Chem. Phys.* **1997**, *107*, 3032.
(19) Zhao, Y.; Truhlar, D. G. *Theor. Chem. Acc.* **2008**, *120*, 215.
(20) Ribero, R. F.; Marenich, A. V.; Cramer, C. J.; Truhlar, D. G. *J. Phys. Chem. B* **2011**, *115*, 14556.
(21) Wheeler, S. E.; Houk, K. N. *J. Chem. Theory Comput.* **2010**, *6*, 395.
(22) (a) Zhao, Y.; Truhlar, D. G. *Phys. Chem. Chem. Phys.* **2008**, *10*, 2813. (b) Ribeiro, R. F.; Marenich, A. V.; Cramer, C. J.; Truhlar, D. G. *J. Phys. Chem. B* **2011**, *115*, 14556.
(23) Cambridge Crystallographic Data Centre as supplementary publication no. 100846. Copies of the data can be obtained free of charge on application to The Director, CCDC, 12 Union Road, Cambridge CB2 1EZ, UK [fax: (int.) +44 (0)1223 336033, e-mail: deposit@chemcrys.cam.ac.uk].
(24) Ess, D. H.; Houk, K. N. *J. Am. Chem. Soc.* **2007**, *129*, 10646.
(25) Yamago, S.; Nakamura, E. *J. Am. Chem. Soc.* **1989**, *111*, 7285.
(26) Woodward, R. B.; Hoffmann, R. *J. Am. Chem. Soc.* **1965**, *87*, 395.
(27) Carpenter, B. K.; Little, R. D.; Berson, J. A. *J. Am. Chem. Soc.* **1976**, *98*, 5723. (b) Platz, M. S.; McBride, J. M.; Little, R. D.; Harrison, J. J.; Shaw, A.; Potter, S. E.; Berson, J. A. *J. Am. Chem. Soc.* **1976**, *98*, 5725. (c) Siemionki, R.; Shaw, A.; O'Connell, G.; Little, R. D.; Carpenter, B. K.; Shen, L.; Berson, J. A. *Tetrahedron Lett.* **1978**, 3529. (d) Nakamura, E.; Yamago, S.; Ejiri, S.; Dorigo, A. E.; Morokuma, K. *J. Am. Chem. Soc.* **1991**, *113*, 3183. (e) Nakamura, E.; Yamago, S. *Acc. Chem. Res.* **2002**, *35*, 867.
(28) Ejiri, S.; Yamago, S.; Nakamura, E. *J. Am. Chem. Soc.* **1992**, *114*, 8707.
(29) (a) Lautens, M.; Klute, W.; Tam, W. *Chem. Rev.* **1996**, *96*, 49. (b) Paquette, L. A. *Top. Curr. Chem.* **1984**, *119*, 1.
(30) Brandi, A.; Cacchi, S.; Cordero, F. M.; Goti, A. *Chem. Rev.* **2003**, *103*, 1213.
(31) Garcia-Fandiño, R.; Gulias, M.; Mascareñas, J. L.; Cardenas, D. J. *Dalton Trans.* **2012**, *41*, 9468.
(32) Suzuki, T.; Fujimoto, H. *Inorg. Chem.* **2000**, *39*, 1113.
(33) Legault, C. Y. *CYLview 1.0b*; Université de Sherbrooke: Sherbrooke, 2014 (www.cylview.org).